Journal of Applied Electrochemistry **34**: 417–426, 2004.

Behaviour, modelling and simulation of a pulsed three-dimensional radial electrode with continuous solid flow: Part I

F.J. GARFIAS-VASQUEZ[1,*], P. DUVERNEUIL[2] and G. LACOSTE[2]
[1]*Facultad de Química, Universidad Nacional Autónoma de México, Cd. Universitaria, México, D.F., 04510*
[2]*École Nationale Supérieure des Ingénieurs en Arts Chimiques et Technologiques, Institut National Polytechnique de Toulouse, 118 Route de Narbonne, 31077 Toulouse Cedex 04, France*
*(*author for correspondence)*

Received 28 January 2001; accepted in revised form 4 November 2003

Key words: electrochemical cell, pulsating flow, three-dimensional electrode

Abstract

A new electrolysis cell, the radial PPPE, in which the solid cathode is able to circulate continuously through the cell by pulsation, is described. The behaviour of the liquid and solid phases is analysed to understand the operation of the cell and the effect of pulsation. Two distinct regions are observed in the solid cathode during the upward pulsation: a stable upper and a destabilized lower region. The circulation in the upper region, segregation in the lower region and exchange between the two regions are characterized experimentally as a function of the maximum fluidizing height bed. Electrodeposition occurs in both regions. The RTD of the solid particles was determined.

1. Introduction

Metal recovery by classical electrochemistry on a planar cathode is widely used in industry for effluents having high dissolved metal concentrations. However, at relatively low metal concentrations, a planar cathode becomes expensive because large electrode surface areas are needed and the current density cannot be increased. To overcome this limitation we used a cathode of a high surface area per unit volume made of granular particles. A previously developed electrode [1] had a fixed bed percolated by the electrolyte; such a configuration was known as the percolated porous electrode (PPE). The PPE had a better performance than a planar cathode because of its higher specific surface area per unit volume and the improved mass transfer behaviour. Consequently, the PPE allowed the use of high current densities to recover dissolved metals from effluents having low concentrations. The main disadvantage of a PPE cell is bed solidification. To overcome this disadvantage, a cell involving pulsation was developed. The cathode of such a cell is known as the pulsed percolated porous electrode (PPPE). The PPPE cell maintained the bed in motion during a fraction of a pulsating cycle, thus preventing the bed from plugging, whereas in the other fraction it was static. Two possible electrical fields are found in PPPE cells with respect to their relative orientation of the liquid flow patterns: 'axial-' and 'cross electric fields'. For a PPPE cell having a cylindrical cathode and anode, the cross electric field is radial.

This paper describes an improvement to the PPPE cell that consists in continuously feeding and extracting the granules from the cell until steady state is reached. The design of this new cell was patented in 1996 [2]. To design this improved cell, the behaviour of the variables affecting the system-flow dynamics and the rate of mass transfer were noted. The phenomena taking place in such a cell are so complex that we proceeded by stages, observing first the system dynamics in a closed pulsed cell with no electrolysis and then determining the particle residence time distribution when particles are fed and extracted at different pulsation rates [3, 4].

2. Dynamic flow pattern equipment

The study was initially undertaken with equipment that mechanically simulated a PPPE cell with a radial field configuration without granules being fed or extracted. To simulate the flow pattern, the electrode configuration was simplified. The equipment used for the dynamic flow studies is shown in Figure 1. It consisted of three principal parts: a cell, a continuous liquid feed system and a pulsating pneumatic system. The cell consisted of three sections: (i) Two external cylindrical walls of transparent Plexiglas 0.6 m high (H) and of diameters $D_1 = 0.3$ m and $D_2 = 0.25$ m, which represents the external cylindrical porous diaphragm of the cell. The chamber between the two walls mimics the external anodic compartment. (ii) An inner Plexiglas cylinder of 0.1 m outside diameter D_3, that mimics the internal

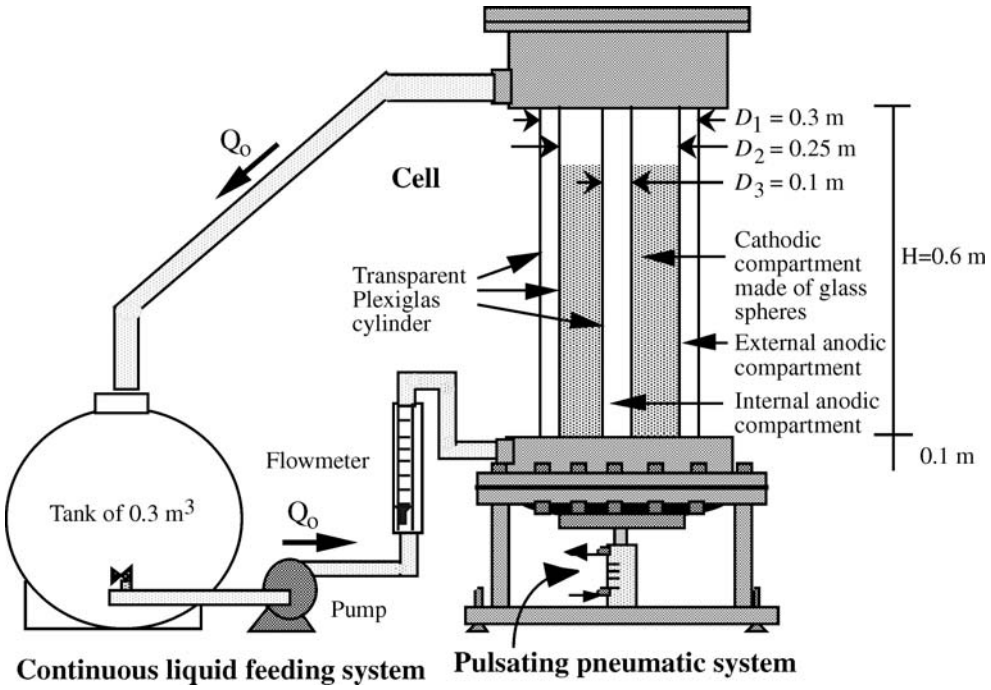

Fig. 1. Experimental PPPE radial cell.

anodic compartment, placed in the centre of the cell. This could be taken out when not needed. (iii) A cathodic compartment delimited by the external and internal anodic compartments. Instead of a cathodic bed made of a conductor or semiconductor material, glass spheres were used that allowed observation of their movement.

The continuous liquid feed system consisted of a pump that fed the liquid into the bottom of the cell through a grid to guarantee uniform liquid distribution. After flowing through the cell, the liquid left the top and entered a storage tank. The pulsating pneumatic system consisted of a piston connected to a disc $D_P = 0.25$ m in diameter, acting on an elastic membrane, which was flanged to a 0.1 m high polyvinyl column 0.5 m internal diameter (D_m). The Polyvinyl column was fixed to the cell and the movement of membrane displaced the liquid. Compressed air acted on the piston, giving a continuous movement to the liquid at the cell bottom. The amplitude (a) and the frequency (f) of pulsation are relevant parameters.

3. Liquid phase behaviour

Increasing the pulsating parameters, a and f, increases the liquid flow. It is only required to relate the piston displacement to liquid flow, as the liquid flow inversion is the same as the piston stroke frequency. Since the membrane is fixed to a column of larger diameter than the cell, the volume of liquid displaced by each pulse was measured without having the internal anodic compartment fixed to the cell.

3.1. *Liquid volume displaced in a stroke*

The pulsating system had a piston of diameter D_p that acted on a membrane of larger diameter D_m. The piston moved up and down in a jack with a vertical displacement h_d, which was changed by sliding a higher fixing knob up or down on the piston column. The lower fixing knob was always kept in the same position. The maximum attainable piston stroke and membrane displacement in the vertical direction was 2λ. To minimize the membrane deformation at the maximum possible piston displacement, the midpoint of the maximum piston stroke was located where the membrane was undistorted, that is, to occur when $h_d = \lambda$. At any other pulsating condition, the lowest point of the piston stroke was kept fixed at $h_d = 0$ as a reference point. If the piston is at position $h_d = 2\lambda$, the membrane takes a truncated cone shape of height λ with the larger diameter equal to the D_m, and the smaller diameter, equal to the D_p. When the piston is at position $h_d = 0$, the membrane rests on the piston, thus resembling the shape of a truncated cone with the smaller diameter in the lowest position. Considering the liquid contained in the truncated cone, the displaced liquid volume (V_L) in relation to the reference position is as follows:

$$V_L = \frac{\pi}{12}\lambda\left(D_m^2 + D_m D_p + D_p^2\right) \quad (1)$$

V_L was also measured in the column. For the cell without internal anodic compartment, V_L in the column with D_2 and height of liquid $h_L = 2a$, is

$$V_L = \frac{\pi}{4} D_2^2 \; h_L = \frac{\pi}{2} D_2^2 a \tag{2}$$

By combining Equations 1 and 2, a may be calculated in terms of the geometry of the pulsating system, the piston movement and D_2. Thus,

$$a = \frac{h_d}{6D_2^2}\left(D_m^2 + D_m D_p + D_p^2\right) \tag{3}$$

To validate Equation 3, the higher fixing knob was located at the following distances from the lower fixing knob: 0.02, 0.03, 0.04, 0.045, 0.05, 0.055, 0.06, 0.065 and 0.07 m. With the cell full of water at a fixed height, the level of the liquid displaced was measured, which corresponds to twice the value of a. It has to be considered that the flow feed (Q_0) is zero. Equation 3 reproduces the experimental results and will predict a once the distance between the knobs is fixed. When the internal anodic compartment is inserted into the cell, D_3 was considered. Then Equations 2 and 3, respectively, become

$$V_L = \frac{\pi}{2}\left(D_2^2 - D_3^2\right) a \tag{4}$$

$$a = \frac{h_d}{6\left(D_2^2 - D_3^2\right)}\left(D_m^2 + D_m D_p + D_p^2\right) \tag{5}$$

3.2. *Pulsating liquid movement with a permanent flow feed*

The operating principle of the PPPE cell rests on the pulsation of the permanent liquid feed velocity U_0. In the initial PPPE cells [5–9], liquid destabilization was made by 'mechanical pulsation' (through a driving rod crank), to produce sinusoidal pulsation. In this new generation of electrochemical cell, liquid pulsation is produced by a 'pneumatic system'. Observation of liquid motion without an internal anodic compartment was made with a video camera at a rate of 24 frames per second. The cell was filled with spherical glass particles of diameter 0.004 m (d_p) and density (ρ_p) 2500 kg m^{-3} for an initial bed height of $h_0 = 0.3$ m. For these experiments, the a and f operating parameters are shown in Table 1. For all operating conditions the piston acceleration and deceleration is very fast, as shown in Figure 2. The liquid instantaneous motion $z_L(t)$, can be described in the two phases of period T, as follows: for the upward and downward motion,

Table 1. Operation parameters for determining liquid motion

Number of experiment	a /m	f /Hz
1	0.033	0.38
2	0.033	0.42
3	0.040	0.30
4	0.045	0.38
5	0.054	0.25
6	0.054	0.30
7	0.060	0.35
8	0.060	0.42

$$z_L^+(t) = -a + \frac{2a}{T/2} t = -a + 4aft \quad (0 < t \leqslant T/2) \tag{6}$$

$$z_L^-(t) = a - \frac{2a}{T/2}(t - T/2) = a - 4af(t - T/2) \quad (T/2 < t \leqslant T) \tag{7}$$

From these expressions, two velocity values for both phases of T are obtained by derivation of liquid instantaneous motion with respect to time:

$$U^+ = \frac{dz_L^+(t)}{dt} = 4af \tag{8a}$$

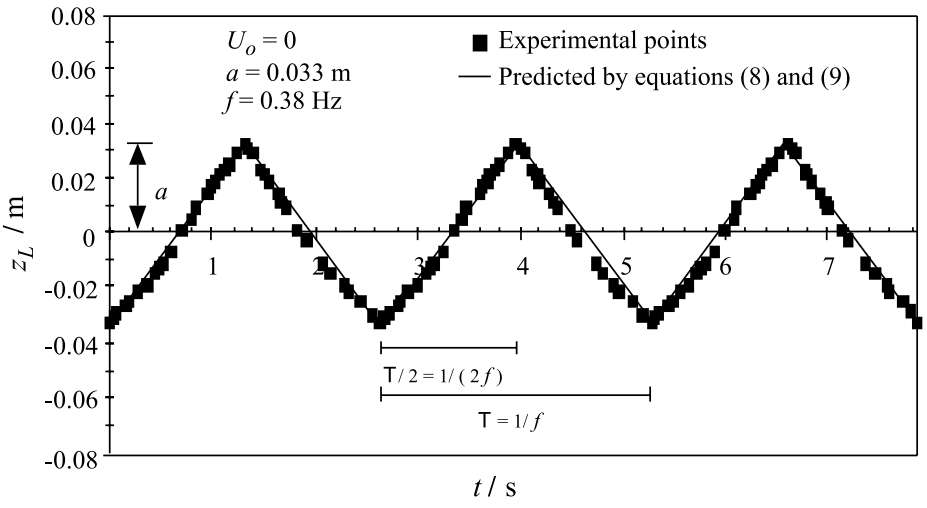

Fig. 2. Vertical profile of liquid motion during pulsation ($U_0 = 0$, $a = 0.033$ m and $f = 0.38$ Hz).

and

$$U^- = \frac{\mathrm{d}z_L^-(t)}{\mathrm{d}t} = -4af \tag{8b}$$

Thus, the pulsating period may be simplified by two constant velocities U^+ and U^- over two equal parts of T. Figure 2 shows a satisfactory correlation with experimental results. By considering U_0, we have, for U^+ and U^-,

$$U^+ = U_0 + 4af \tag{9a}$$

and

$$U^- = U_0 - 4af \tag{9b}$$

with $U_0 = 4Q_0/\pi D_2^2$. The behaviour is illustrated in Figure 3. $z_L(t)$ becomes

$$z_L^+(t) = -a + (4af + U_0)t \tag{10a}$$

and

$$z_L^-(t) = a + (-4af + U_0)(t - T/2) \tag{10b}$$

At the end of a pulsation, the level of liquid displaced is U_0T.

4. Solid phase behaviour

4.1. *Non-stationary transition from a fixed to a fluidized bed*

If U is suddenly increased in a bed of a fixed height h_0 in a stationary state, the bed becomes fluidized and decompression occurs that moves upwards from the bottom of the bed. The velocity of the decompression wave (U_d) occurs at the transition between the fixed state and the fluidized state. The time for acceleration and deceleration is of the order of 10^{-2} to 10^{-4} s. It may be assumed that the particles move with a constant velocity U_d immediately after a perturbation due to the shortness of the transition [11, 12], which is

$$U_d = \sqrt{3.2gd_p, (1-\varepsilon)(\rho_p - \rho)/\rho_p} \tag{11}$$

For particles with similar density to the liquid [13]:

$$U_d = \frac{k_r U + \sqrt{k_e(1+k_r) - k_r U^2}}{1 + k_r} \tag{12}$$

where $k_e = 2[3.2\,g\,d_p(1-\varepsilon)(\rho_p - \rho)]/(2\rho_p + \rho)$ and $k_r = 3[(1-\varepsilon)/\varepsilon]\rho/(2\rho_p + \rho)$. The void fraction and liquid velocity values for the bed decompression are $\varepsilon = \varepsilon_0$ and $U = U_{mf}$, respectively. If the upward flow is suddenly stopped, and consequently the bed decompresses, the bed reaches a 'maximum fluidizing height' (h_{max}). Considering the bed decompression time (t_d), h_{max} can be expressed as

$$h_{max} = U_d t_d \tag{13}$$

4.2. *Experimental determination of h_{max}*

As the conductivity between any two points depends on the distance and the number of nonconductive particles present, the electrical conductivity method was used for the experimental determination of h_{max} [14, 15]. The

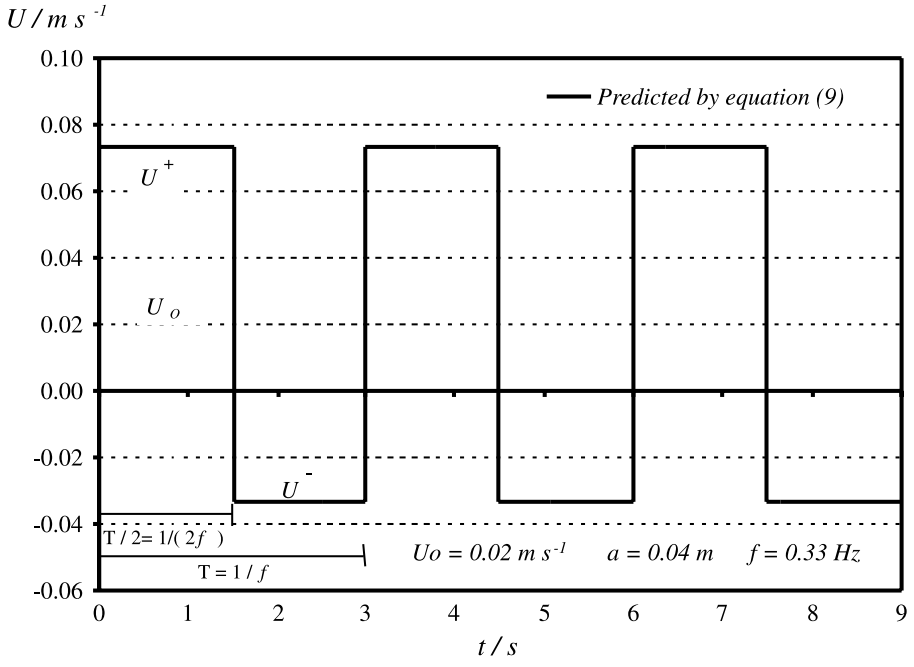

Fig. 3. Representation of liquid velocities during pulsation.

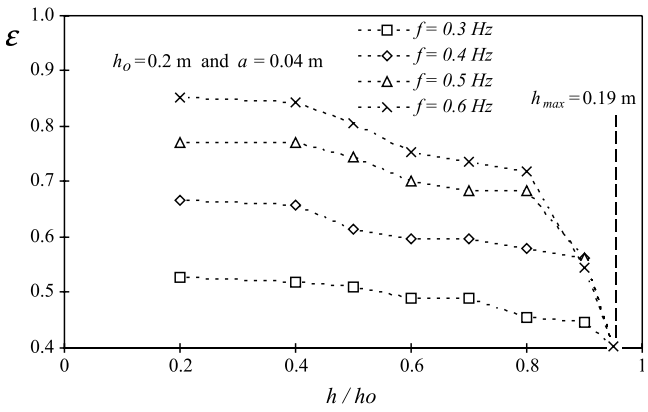

Fig. 4. Evolution of maximum voidage as a function of fractional bed height h/h_0 for different pulsation frequencies: 0.04 m amplitude and 0.2 m bed height. Key1 for *f*: (□) 0.3, (◇) 0.4, (△) 0.5 and (×) 0.6 Hz. $h_0 = 0.2$ m and $a = 0.04$ m.

experimental equipment was similar to that shown in Figure 1. The experimental determination of h_{max} was made for different h_0, a and f. For each set, the electrical apparent conductivity (κ) of the potassium chloride solution (KCl) of known concentration was measured when the bed was pulsed by the liquid. One probe was located in the centre of the bed and the other was set up close to the wall. The probes were 0.8 m in height. The probes were placed at different heights in the bed to measure κ. When κ of the KCl solution is known at the two extremes (i.e., the fixed bed and the total fluidized bed), then the vertical value along the bed of the maximum ε for fixed a, f and h_0 can be deduced. This value represents U_d. In the first experimental series, in which operating conditions were: $a = 0.04$ m and $h_0 = 0.2$ m, it was observed for all different operating f, that ε became equal to $\varepsilon_0 = 0.4$ from $h_{max} = 0.19$ m to the final height bed h_f. It must be said that the ε value of 0.4 corresponds to the voidage value of a fixed spherical particle bed, as shown in Figure 4. For the other experimental series, the same observations were made, ε being 0.4 as soon as the value of 0.18–0.20 m was reached for h_{max}. The experimental results for a, f and h_0 are shown in Table 2. The height h_{max} defines two regions with different behaviour: a destabilized bed in the *lower* region of height h_{max} and ε value lying between $0.4 < \varepsilon < 1$ and a stable bed in the *upper* region with a ε value equal to the void fraction of a fixed bed and a height, h_A, that is a function of the h_0. The height of the lower region during the downward motion of the piston had the value h_B. Both regions during the upward and the downward motions of the piston are shown graphically in Figure 5.

4.3. *Particle circulation*

Knowledge of particle exchange between the stable and destabilized regions is required for precise scale-up of the PPPE radial cell. The global upward velocity U_p^+ of the fixed bed was calculated by the equation proposed by Slis et al. [16] and modified by Gibilaro et al. [11], $U_p = U_f - U_i$, where U_i and U_f are the initial and the final liquid velocity during the upward motion of the bed. Considering that the movement of the fixed bed starts when $U > U_{mf}$, and U_f is calculated by the Equation (9), then U_p^+ and U_p^- can be written as

$$U_p^+ = U_0 + 4af - U_{mf} \tag{14a}$$

and

$$U_p^- = U_0 - 4af - U_{mf} \tag{14b}$$

The final height h_f of the bed during the expansion at the upper time ($T/2$) can be described in terms of h_0 and the upward motion of the upper region (z_p^+), using U_p^+ gives

$$h_f = h_0 + z_p^+ = h_0 + U_p^+ T/2 \tag{15}$$

At the *lower* region of the bed, a new bed void fraction ε_1 is generated. It should be the same as ε when total expansion by U^+ is reached. This was calculated for spherical particles by Riba and Couderc [17]. U_d can determine the height of the lower region corresponding to h_{max} during pulsation. U_d for $t_d = T/2$, with the Equations 11 and 12, where $U = U^+$, the h_{max} becomes

$$h_{max} = U_d T/2 \tag{16}$$

The height of upper (h_A) and lower (h_B) regions are expressed by

Table 2. Experimental and calculated values h_{max}, h_f, h_A and h_B for $h_0 = 0.5$ m

a /m	f /Hz	U^+ /ms^{-1}	h_{max} /m	h_{max} /m	h_f /m	h_A /m	h_B /m
			Experimental	Calculated			
0.04	0.4	0.064	0.18	0.235	0.526	0.291	0.209
	0.5	0.08	0.18	0.193	0.537	0.344	0.156
	0.6	0.096	0.18	0.164	0.544	0.38	0.12
0.06	0.4	0.096	0.2	0.248	0.566	0.318	0.182
	0.5	0.12	0.2	0.204	0.577	0.373	0.127
	0.6	0.144	0.2	0.174	0.584	0.41	0.09

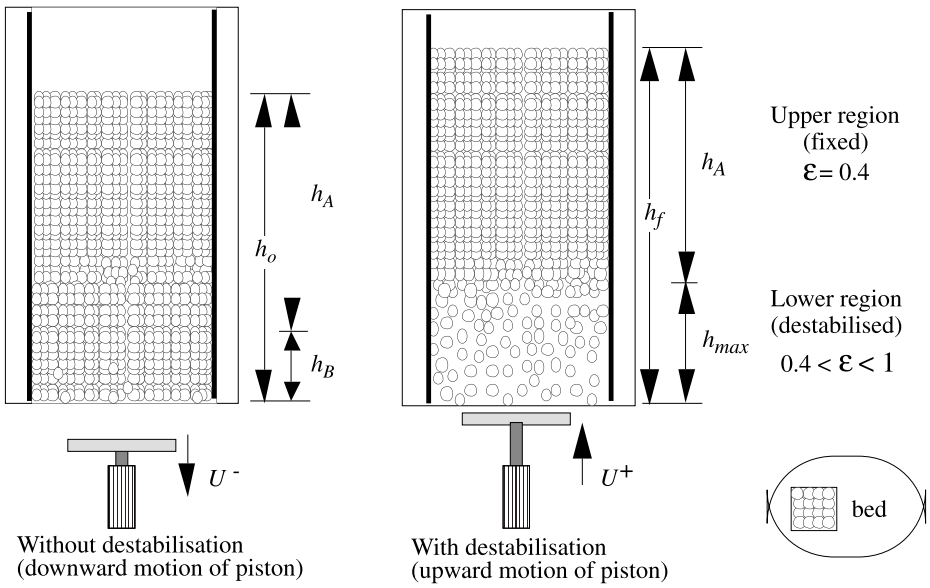

Fig. 5. Solid phase behavior of porous PPPE radial cell.

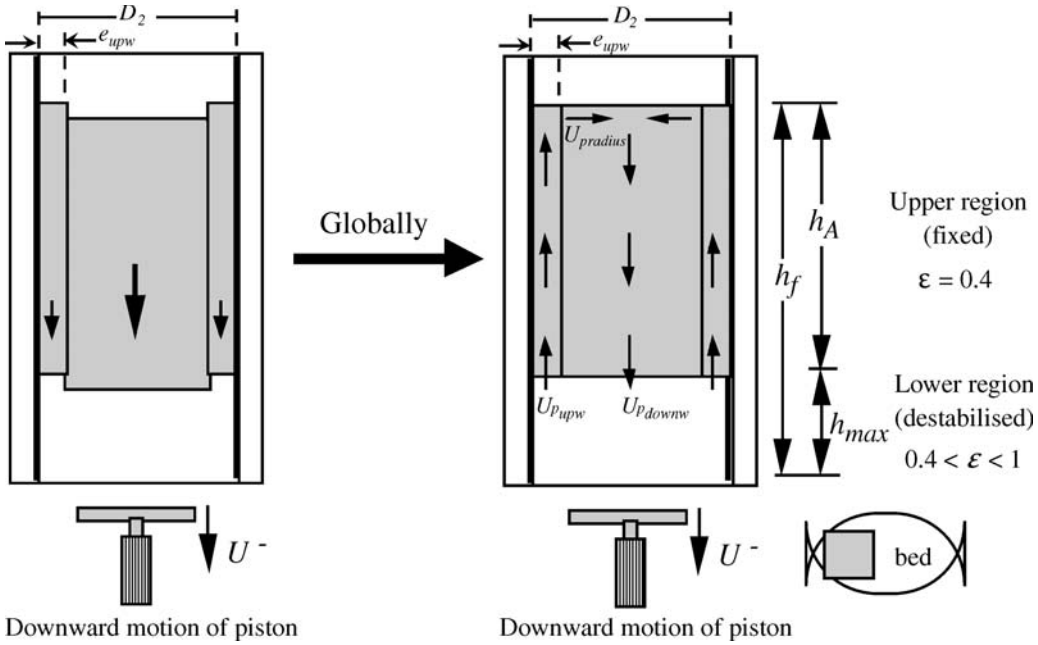

Fig. 6. Solid phase behavior of porous PPPE radial cell at the upper zone.

$$h_A = h_f - h_{max} \text{ and } h_B = h_0 - h_A \quad (17)$$

The experimental and calculated values of h_{max} by the Equation 16 as well as the calculated values of h_f, h_A and h_B by the Equations 15 and 17 are given in Table 2. From these results, it can be said that for same a, the calculated h_{max} decreases with an increment of the operating f and, consequently, there is an increase in h_A; and for the same f, h_{max} increases slightly with a accompanied by an increase in h_A. The h_{max} values calculated by Equation 16 represent the observed values.

4.4. *Characterization of particle circulation in the upper region*

As the piston moves downward at constant velocity, the upper region in block moves accordingly. Two different zones are then observed (Figure 6): a *central zone* in the core of the bed with a downward movement equal to the movement of the piston and a 'border zone' of particles close to the rough wall with thickness e_{upw}, where the velocity is smaller than in the central zone. Altogether, an upward movement of particles is observed close to the wall, where the electrochemical reaction takes place.

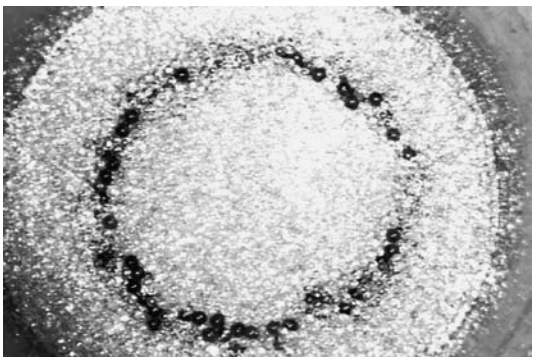

Fig. 7. Photograph of marked particle layer at 0.36 m bed height. Operating conditions: $h_o = 0.4$ m, $a = 0.06$ m, $f = 0.6$ Hz and operation time of $t = 30$ s.

The knowledge of circulation velocities and volume of each zone allows the residence time in each zone to be determined. To determine the velocities, as well as the thickness e_{upw} of the upward particles close to the wall, some particles were marked and followed. The upward motion of marked particles was filmed and was analysed layer by layer to determine the position of the marked particles, which move from the top to the centre of the bed. In Figure 7, a layer of marked particles is shown with a downward motion at the centre of the bed. By measuring the position for different a and f, the circulation velocities are determined for particles with: an upward motion close to the wall (Up_{upw}), a movement from the top to the centre of the bed (Up_{radius}) and a downward motion at the centre of the bed (Up_{downw}). The obtained values of experimental velocities are given in Table 3. Up_{upw} increases rapidly with a or f. Velocities can be ranked in the order: $Up_{upw} > Up_{radius} > Up_{downw}$. The residence time for a particle is smaller in the zone close to the wall than in the rest of the upper region. The upward and downward volumetric flow of particles in the PPPE cell determines the flow of particles with a thickness of e_{upw} close to the rough wall. The volumetric flows of particles are expressed as

$$Q_{upw} = \Omega_{upw}\ Up_{upw} = \frac{\pi}{4}\left[D_2^2 - (D_2 - 2e_{upw})^2\right] Up_{upw} \tag{18}$$

$$Q_{downw} = \Omega_{downw}\ Up_{downw} = \frac{\pi}{4}\left(D_2 - 2e_{upw}\right)^2 Up_{downw} \tag{19}$$

As in a closed system, the two volumetric flows are equal, the thickness e_{upw} was obtained from Equations 18 and 19:

$$\left(Up_{upw} + Up_{downw}\right)e_{upw}^2 - D_2\left(Up_{upw} + Up_{downw}\right)e_{upw} + \left(\frac{D_2}{2}\right)^2 Up_{downw} = 0 \tag{20}$$

This equation has two positive roots as solutions. From Equation 20, the positive roots for $Up_{upw} = 0.037 \times 10^{-2}\,\mathrm{m\,s^{-1}}$ and $Up_{downw} = 0.01 \times 10^{-2}\,\mathrm{m\,s^{-1}}$ are 0.236 and 0.0141 m. As $e_{upw} < D_2/2$, then it could be that $e_{upw} = 0.0141$ m.

For different a and f, the e_{upw} of particles with upward motion close to the wall is in the zone of 0.015 m, shown in Table 3. This value compares well to the value reported by Takahashi and Yanai [18] for a cylindrical bed 0.1 m in diameter. Finally, the experimental values of Up_{upw} in the upper region could be related to velocity U^+ by the Equation 9 as a function of U_{mf} [10]:

$$\frac{Up_{upw}}{U_{mf}} = 0.110\left(\frac{U^+}{U_{mf}}\right)^2 - 0.182\frac{U^+}{U_{mf}} + 0.072 \tag{21}$$

In Figure 8, a comparison is made between the experimental and calculated values (Equation 21). It should be pointed out that for U^+ lower than U_{mf}, Up_{upw}

Table 3. Experimental results of particle circulation velocities

a /m	f /Hz	U^+ /m s^{-1}	Up_{upw} /m s^{-1}	Up_{radius} /m s^{-1}	Up_{downw} /m s^{-1}	e_{upw} /m
0.03	0.33	0.040	0.00037	0.00011	0.00010	1.41
	0.37	0.044	0.00049	0.00068	0.00010	1.1
	0.45	0.054	0.00162	0.00088	0.00039	1.28
	0.50	0.060	0.00245	0.00112	0.00085	1.73
0.04	0.25	0.040	0.00049	0.00013	0.00015	1.56
	0.30	0.048	0.00151	0.00076	0.00049	1.64
	0.35	0.056	0.00248	0.00084	0.00089	1.78
	0.40	0.064	0.00399	0.00157	0.00113	1.46
	0.45	0.072	0.00546		0.00144	1.38
0.06	0.17	0.041	0.00057	0.00024	0.00017	1.53
	0.20	0.048	0.00240	0.00120	0.00069	1.48
	0.30	0.072	0.00570	0.00260	0.00173	1.55
	0.35	0.084	0.00860	0.00319	0.00222	1.36
Average						**1.5**

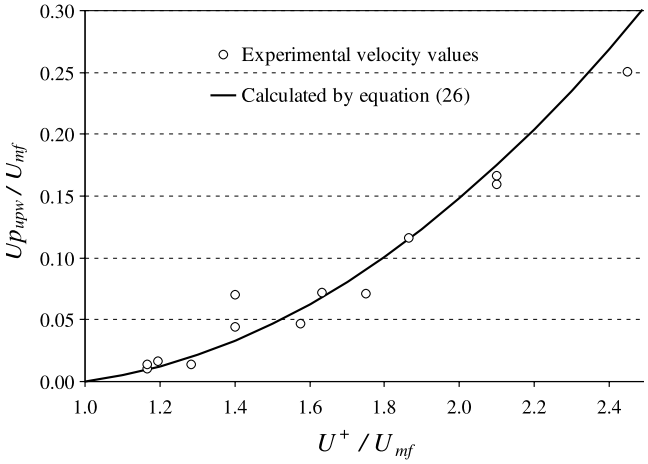

Fig. 8. Comparison of experimental and calculated velocity values.

is equal to zero and increases with U^+. For the lower region, the concentration of particles is almost homogeneous.

5. PPPE cell behaviour with solid feeding

The movement of the solids in this closed operation (batch or discontinuous) with pulsation was followed by the periodic feeding and extraction of granules from the cell.

5.1. *Description of the modified solid movement PPPE cell*

The PPPE cell with radial configuration and continuous operation shown in Figure 9 is made up of six parts: (i) A cathodic compartment delimited by two cylindrical porous polyethylene diaphragms 2 mm thick with $D_2 = 0.28$ m and $D_3 = 0.122$ m, and $H = 0.6$ m. The h_0 is fixed at 0.4 m, as determined by the position of the feeding granule unit. The volume occupied by the fixed bed V_{bed} is 20 300 cm^3. The bed is constituted by carbon granules of petroleum coke of $d_P = 0.0035$ m and $\rho_p = 1700\,kg\,m^{-3}$. (ii) An external anodic compartment delimited by a polyvinyl cylindrical wall cell ($D_1 = 0.3$ m) and a polyethylene cylindrical porous diaphragm ($D_2 = 0.28$ m). An anode 0.1 m in diameter and 0.6 m in height delimited by a polyethylene cylindrical porous diaphragm ($D_3 = 0.122$ m) was placed at the centre of the cell. (iii) A feeding granule unit placed at the top of the cell. This system feeds the virgin granules, maintaining a constant volume of granules in the cell. The lower part of this system is made according to the patent of INPT [2]. (iv) An extracting granule unit is placed at the bottom of the bed at the level of the grid in the lowest part of the column. This system allows setting of the extracting frequency of granules as well as the extracting volume for each operation. (v) The continuous liquid feeding and (vi) the pulsating pneumatic system were described in Section 2.

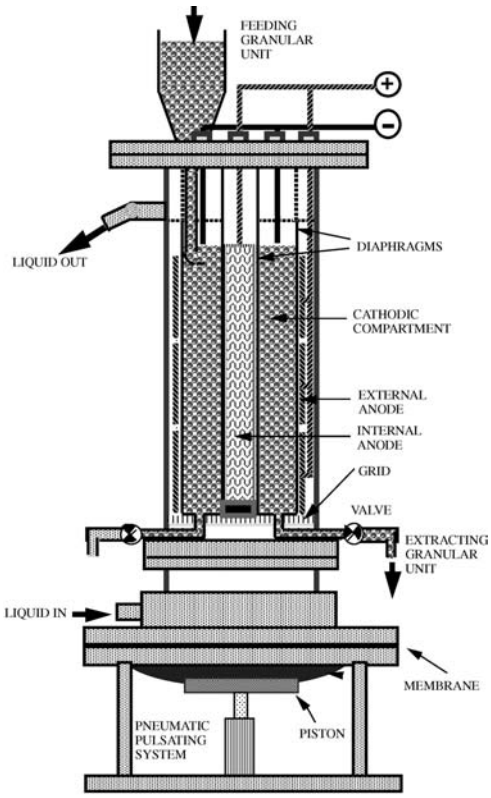

Fig. 9. PPPE radial cell with granules feed and extraction units.

5.2. *Residence time distribution (RTD) of solids in a PPPE cell*

Particles in the column follow different routes as a function of the phenomena that generate this movement (circulation in the upper region, segregation in the lower region and exchange between these two regions as a function of h_{max}). Some particles leave the column very rapidly, while others are able to remain much longer in the bed. The good behaviour of the process (desirable characteristics of final product) depends on the residence time (t_s) of the particles in the cell.

Our objective is to determine the RTD experimentally and to calculate the curve $F(\theta)$ for the solid in the bed during continuous operation of the PPPE cell. The particles introduced at the top of the bed have a precise t_s in each region of the cell; t_s is an essential parameter to determine the amount of metal deposited on the particles during operation. Factors that destabilized the bed by pulsed flow were: U_0, a, f when U_0 is smaller than U_{mf}. The U_{mf} is estimated from the physical properties of a liquid–solid system with $\mu = 0.001$ Pa s, $\rho = 1000\,kg\,m^{-3}$, $\rho_p = 1700\,kg\,m^{-3}$, $d_p = 3.5 \times 10^{-3}$ m; then U_{mf} is $2 \times 10^{-2}\,m\,s^{-1}$. U_0 is fixed at $0.4 \times 10^{-2}\,m\,s^{-1}$. h_d is fixed between 0.02 and 0.1 m. From Equation 5, a was found to be 0.035 m. The experiments were carried out for $f = 0.24$, 0.3 and 0.33 Hz to ensure that a liquid velocity inversion took place.

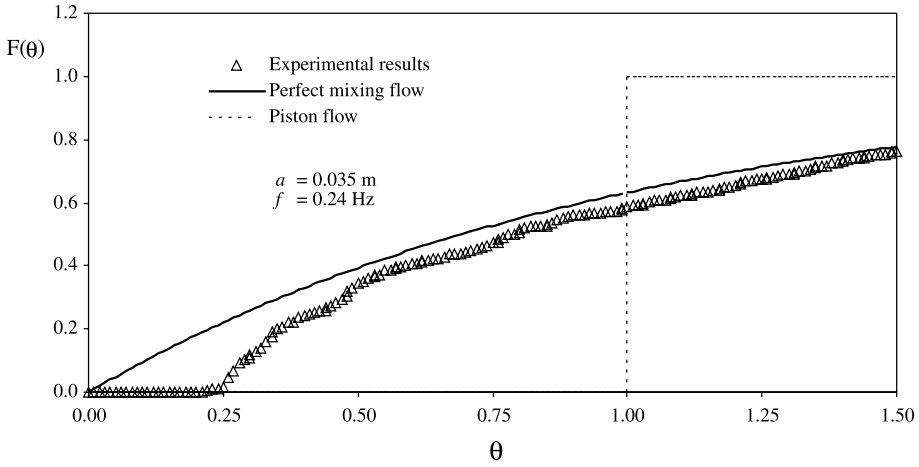

Fig. 10. RTD for PPPE radial cell with solid flow ($a = 0.035$ m and $f = 0.24$ Hz).

At the start, a tracer signal ($N_0 = 1000$ particles) was introduced at the top of the bed by the feeding unit. The feed tracers rested long enough to maintain the bed stable. The RTD was determined by counting the number of tracers N_s found in the extracting granule unit. In two experiments, the extraction was 200 and 500 $cm^3\,h^{-1}$. The number of accumulated tracers N was counted in the extracting granule unit. The function $F(\theta)$, which represents the fraction of tracers N/N_0 out of the cell, was calculated and compared with the theoretical function $F(\theta)$ for an ideal mixed cell, $F(\theta) = 1 - \exp(-\theta)$ and $\theta = t_s/t_g$, where t_g and θ are the geometric time and reduced residence time of the particles, respectively. t_g is the ratio between the solid flow Q_{solid} and V_{bed}. For an ideal piston cell, the function $F(\theta)$ is equal to zero when $\theta < 1$ and $F(\theta)$ is equal to 1 when $\theta \geqslant 1$.

5.3. *Results and conclusions*

Three experiments were carried out in the PPPE. For the first experiment at $U^+ = 2U_{mf}$ in 67 h, the first tracers appeared at 8 h in the extracting unit (Figure 10), which corresponds to $\theta = 0.25$. Then the experimental results begin to approach the theoretical curve represented by perfectly mixed behaviour. It was also observed that PPPE behaviour becomes similar to a mixed cell with an 8 h delay caused by the initial distance, as the granules have to cover the upper region of the bed. For the second experiment with both a higher liquid pulsating velocity ($U^+ = 2.3\,U_{mf}$) and higher f, the first tracers appeared 4 h later. Then a similar behaviour was observed as in the preceding determination. The analysis of the experimental results also shows a mixed behaviour, where t_s becomes shorter for the upper region. In the third experimental run with $U^+ = 2.5\,U_{mf}$, maintained for 58 h and carried out at different operating conditions in the extracting granule unit, the first tracers appeared after 1 h. The cell also showed a mixed behaviour. In the three experiments, it was observed that the global behaviour of the PPPE radial cell corresponded to a mixed cell. The decrease in the extracting flow over the RTD showed an increase in t_s. This model can be used to establish the movement and extracted volume of granules since the solid phase behaviour corresponds to a mixed cell.

6. General conclusions

It is observed that the flow dynamics consisted of an upward and downward movement at constant speed, which can be expressed as a function of a, f of pulsation and U_0. For the solid phase, two zones were evident: a lower region of height h_{max}, where the bed is destabilized with an ε value lying between 0.4 and 1 and an upper region where the bed remains compacted with an ε value of 0.4 equal to that of a fixed bed. It is shown that the height h_{max} is independent of pulsation and of h_0. The upper region, even when not destabilized, had a particle circulation with an upward movement at the outer portion and a downward movement at the centre of the bed. The PPPE cell behaves like a perfectly mixed cell whenever U^+ is at least twice U_{mf}. A perfectly mixed cell has the advantage of producing particles with uniform physical parameters.

Acknowledgements

This work was supported by the Mexican institutions Consejo Nacional de Ciencia y Tecnología (CONACYT) and by Dirección General de Asuntos del Personal Académico from the Universidad Nacional Autónoma de México (UNAM).

References

1. G. Lacoste and H. Olive, Institut National Polytechnique de Toulouse (INPT) – Kodak Pathé, European patent 814 004 693 (1984).

2. G. Lacoste and P. Duverneuil, INPT – Kodak Pathé, International patent WO 9 700 398 (1997).
3. F.J. Garfias-Vásquez, P. Duverneuil and G. Lacoste, *in* I. Rousar., 'Contemporary Trends in Electrochemical Engineering' (Prague, 1996), p. 316.
4. F.J. Garfias Vásquez, Thèse de Doctorat, INPT, France (1997).
5. A. Ratel, Thèse de Doctorat, INPT, France (1987).
6. A. Gadri, A. Ratel and G. Lacoste, *J. Appl. Electrochem.* **28** (1998) 921.
7. D. Molina, Thèse de Doctorat, INPT, France (1991).
8. F. Massy, Thèse de Doctorat, INPT, France (1991).
9. J. Rodrigues de Souza, Thèse de Doctorat, INPT, France (1993).
10. J.P. Riba, R. Routie and J.P. Couderc, *Can. J. Chem. Eng.* **56** (1978) 26.
11. L.G. Gibilaro, P. Waldram and P.U. Foscolo, *Chem. Eng. Sci.* **39** (1984) 607.
12. P.U. Foscolo and L.G. Gibilaro, *Chem. Eng. Sci.* **42** (1984) 1667.
13. L.G. Gibilaro, R. Di Felice and P.U. Foscolo, *Chem. Eng. Sci.* **45** (1990) 1561.
14. P.N. Rowe and H. Masson, *Trans. Inst. Chem. Eng.* **59** (1981) 177.
15. J.S. Halow and P. Nicoletti, *Powder Technol.* **69** (1992) 255.
16. P.L. Slis, Th.W. Willemse and H. Kramers, *Appl. Sci. Res.* **8** (1959) 209.
17. J.P. Riba and J.P. Couderc, *Can. J. Chem. Eng.* **55** (1977) 118.
18. H. Takahashi and H. Yanai, *Powder Technol.* **7** (1973) 205.